JOURNAL OF MATERIALS SCIENCE 24 (1989) 1772–1776

The use of linear elastic fracture mechanics for particulate solids

M. J. ADAMS, D. WILLIAMS
Unilever Research, Port Sunlight Laboratory, Quarry Road East, Bebington, Wirral, Merseyside, L63 3JW, UK

J. G. WILLIAMS
Department of Mechanical Engineering, Imperial College, Exhibition Road, London SW7 2BX, UK

The fracture of model porous particulate solids consisting of sand and low volume fractions of a polymeric binder has been investigated. In order to apply a linear elastic fracture mechanics analysis it was necessary to use an effective crack length comprising the sum of the notch depth and a quantity Δa. The behaviour of the model solids was intermediate between that exhibited by ceramics and polymers. A possible interpretation of Δa is that it represents a process zone size where the energy dissipation mechanism could involve either microcracking or yielding of the interparticle junctions in the zone. The former would correspond to ceramic-like behaviour while the latter is characteristic of polymers.

1. Introduction

There are a number of industries where the strength of relatively porous particulate solids is critical during manufacture. Typical products include metallic and ceramic green compacts [1], pharmaceutical tablets [2] and particulate granules [3]. Often in these technological fields, the strength is expressed in terms of a nominal stress using, for example, diametric compression of a cylindrical specimen. Such an approach has many limitations, as in many other fields, it is more satisfactory to apply linear elastic fracture mechanics (LEFM) and in the current work such an approach was considered for a model particulate solid comprising sand and a polymeric binder polyvinylpyrrolidone (PVP). However, difficulties were experienced which were analogous to those found in attempts to apply LEFM to dense particulate solids such as cement and finished ceramics where sample size effects [4], rising crack resistance curves [5] and differences between initiation and propagation values of the fracture surface energies [6] have been observed.

The strength of materials is usually measured in plane strain because for this condition the fracture parameters are independent of the specimen size. To ensure that plane strain fracture occurs, the geometry of the specimen has to satisfy the following criteria [7]

$$B,\ D/2 > 2.5(K_c/\sigma_y)^2 \quad (1)$$

where B is the specimen thickness and D is the depth (see Fig. 1), σ_y is the yield stress and K_c is the critical stress intensity factor. Experimentally K_c can be obtained from the fracture stress σ of notched or pre-cracked specimens using the following equation

$$K_c = Y\sigma a^{1/2} \quad (2)$$

where a is the notch depth and Y is a polynomial function of a/D which depends on the geometry and loading of the body [8].

The origin of the limits given by Expression 1 is that deviations from plane strain occur when the size of the plastic zone at the crack tip becomes comparable to the specimen dimensions. This leads to a significant component of stress relief at the specimen surfaces (plane stress in the limit) and the fracture parameters then become a function of sample size (e.g. [9]).

The linear elastic Equation 2 is only applicable if the zone size is small compared with the crack length. For ductile materials Irwin [10] showed that it was possible to compensate for limited crack tip yielding by replacing the crack length by an effective length $\tilde{a}$, thus

$$\tilde{a} = a + \Delta a \quad (3)$$

where $\tilde{a}$ was taken to extend to the centre of the plastic zone which has a radius Δa. The quantity Δa is given by $K_c^2/\pi\sigma_y^2$.

In the current work we consider how the Irwin approach can be adopted for the type of particulate solids of interest here. The exact interpretation of Δa for such materials is a matter of some conjecture but as in ductile materials it is a key parameter that prescribes the toughness.

2. Experimental procedure

The bars were prepared by mixing 10 parts of a sieved fraction of angular sand with one part of an aqueous solution of PVP (ex. BDH). The fractions of sand investigated had mean particle diameters of 60, 230 and 300 μm; in some cases mixtures of 60 and 300 μm sand were used in a 1 : 1 proportion. Two molecular weights of PVP, 4.4×10^4 and 7×10^5, were used with the concentrations of the aqueous solutions adjusted to give a weight fraction of PVP in the bars of either 1 or

0022–2461/89 $03.00 + .12

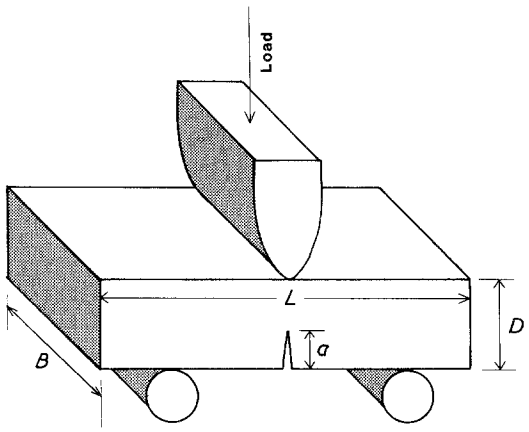

Figure 1 Schematic diagram of the three-point bend configuration used to fracture the specimens where L is the length, B the thickness, D the depth and a the notch length.

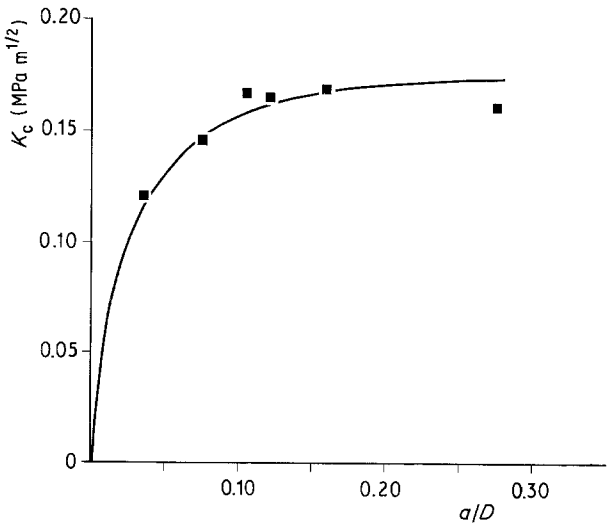

Figure 2 The stress intensity factors K_c as a function of a/D for set E calculated from Equation 2.

2%. The details of each type of bar prepared are given in Table I. The mixture was transferred to a demountable aluminium mould which could accommodate a razor blade in the centre of the base such that a through-thickness notch would be formed in the bar, the height of the blade could be adjusted to give different notch depths. The release of a bar was assisted by previously spraying the inside of the mould with a PTFE release agent and covering the base with a thin PET film. The bars were compressed to a uniform height using an Instron tensiometer (Model 6022); this height was varied in some experiments to obtain different porosities. The nominal dimensions of the bars were 110 (length L) × 21 (thickness B) × 14.8 – 18.5 mm (depth D). The bars were dried in a vacuum oven at 90° C for 1 h before being removed from the moulds. They were then dried for a further 30 min and stored in a desiccator.

At ambient humidities the PVP becomes plasticized by absorbed moisture and at sufficiently high humidities the bars become soft. To ensure that the PVP remained in the glassy state, the bars were sealed in plastic bags and placed in solid CO_2 ice for 4 h prior to testing. The bars were then fractured on the Instron tensiometer using a conventional three-point bend configuration (see Fig. 1); the displacement velocity was fixed at 1 mm min^{-1}. Generally for each type of bar, two unnotched and seven notched ($a/D < 0.4$) were tested.

3. Results and data analysis

In addition to the stress intensity factors, the strain energy release rate G_c was calculated for each specimen. This is related to K_c by the following expression

$$G_c = K_c^2(1 - \nu^2)/E \quad (4)$$

where ν is Poisson's ratio taken as 0.2 for these porous systems and E is Young's modulus which was calculated using the elastic beam equation.

Each set exhibited a range of fracture stabilities depending on the notch size. Usually only the bars with the shortest notches were unstable. At higher notch lengths, unstable fracture with crack arrest occurred and at the highest notch lengths there was completely stable fracture. In each case the initiation value of the strain energy release rate G_{ci} was calculated from the following equation

$$G_{ci} = U_i/BD\phi \quad (5)$$

where U_i is the energy to initiate fracture (taken at the point of maximum force) and ϕ is a calibration factor which is a function of a/D and L/D [11]. For the bars which exhibited stable or unstable fracture with crack arrest, the propagation value of the strain energy release rate G_{cp} was calculated from the total fracture energy U_p as follows

$$G_{cp} = U_p/B(D - a) \quad (6)$$

The trends in the data for all the types of bars studied were similar. Initially we will consider in some detail the data from one of the types (coded set E). They comprised 60 μm diameter sand particles and 2% PVP of molecular weight 7×10^5.

To illustrate the problems of applying a simple linear analysis, Fig. 2 shows a plot of K_c as a function

TABLE I Compositions, particle sizes (d_p) and mechanical results where n represents the final iterated value

Set code	d_p (μm)	PVP MW	Conc. PVP (% w/w)	Porosity	E (GPa)	$K^{(n)}$ (MPa m$^{1/2}$)	$G_{ci}^{(0)}$ (J m^{-2})	$G_{ci}^{(n)}$ (J m^{-2})	$G_{cp}^{(0)}$ (J m^{-2})	$G_{cp}^{(n)}$ (J m^{-2})	$(G_c)_{calc}$ (J m^{-2})	Δa (mm)
A	300	7×10^5	2.0	0.44	2.78	0.34	24.9	43.5	61.4	63.0	44.3	1.0
B	300	7×10^5	2.0	0.54	0.12	0.01	1.2	1.8	3.7	3.8	1.1	0.7
C	300	4.4×10^4	2.0	0.44	1.37	0.10	4.9	10.2	11.7	12.2	7.8	1.5
D	230	7×10^5	1.0	0.43	1.57	0.16	15.3	23.0	30.5	31.0	17.4	0.7
E	60	7×10^5	2.0	0.51	1.76	0.20	13.6	26.3	26.9	30.3	24.4	1.2
F	60/300	7×10^5	1.0	0.44	3.00	0.20	7.8	15.6	19.49	21.1	13.8	1.1
G	60/300	4.4×10^4	2.0	0.43	2.75	0.19	9.1	13.4	15.1	16.4	13.7	1.0

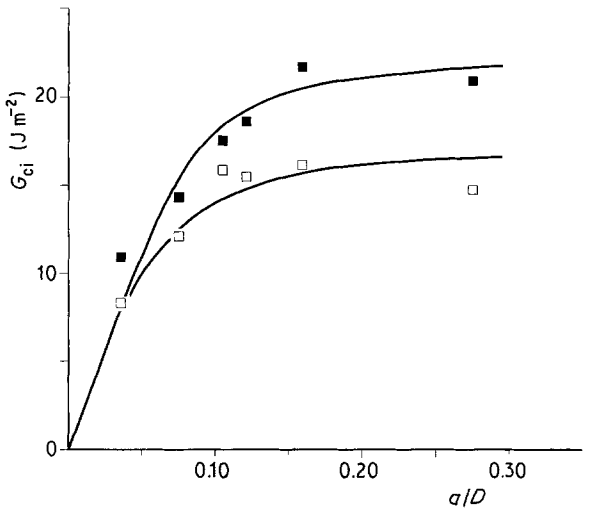

Figure 3 The initiation values of the strain energy release rate G_{ci} as a function of a/D for set E; □ and ■ correspond to the values obtained from Equations 4 and 5 respectively.

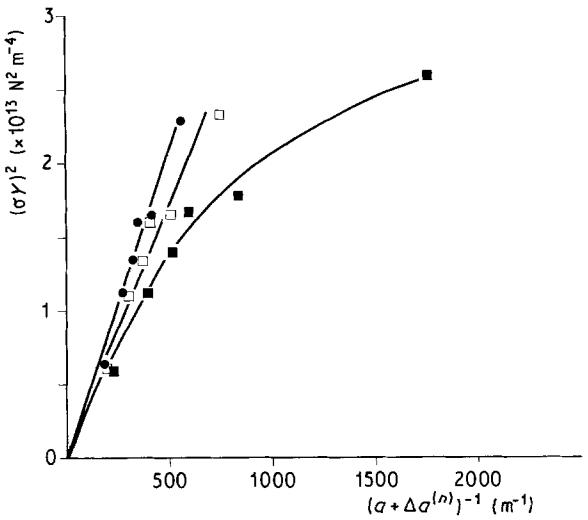

Figure 4 Plots of $(\sigma Y)^2$ as a function of $1/a$ (■), $1/\tilde{a}^{(1)}$ (□) and $1/\tilde{a}^{(6)}$ (●) for set E.

of a/D calculated using Equation 2. The K_c values should be independent of a/D but in fact they range from 0.12 MPa m$^{1/2}$ at the lowest notch depth to 0.17 MPa m$^{1/2}$ at the highest. The corresponding values of the strain energy release rate G_{ci} have similar trends as shown in Fig. 3 where the range is 10.9 to 20.9 J m^{-2}. The calculated values of G_{ci} from Equation 4 also increase with a/D from 8.3 to 14.7 J m^{-2} and are less than the measured values (see Fig. 3).

We will now consider how the introduction of a notional crack length accounts for the apparent non-linearities. This can be achieved by the use of an iterative procedure either for the K_c or G_c values but the former is actually more sensitive. The first stage of the procedure involves plotting $(\sigma Y)^2$ as a function of $1/a$ where $Y = Y(a)$. This produces the curved line in Fig. 4. The initial slope of this curve is used to calculate a first estimate of the K_c value ($K_c^{(0)}$) using Equation 2. Substitution of $K_c^{(0)}$ into this equation with $Y = 1.12\pi^{1/2}$, which is the value for a surface crack in a semi-infinite plate, and the value of σ for an unnotched bar enables a first estimate of Δa to be obtained which is written as $\Delta a^{(0)}$.

The second stage in the iteration is to plot $(\sigma Y)^2$ as a function of $1/\tilde{a}^{(1)}$, which is given by $(a + \Delta a^{(0)})^{-1}$, with $Y = Y(\tilde{a}^{(1)})$. At this stage the plot is linear and a more accurate value of the stress intensity factor, $K_c^{(1)}$, is obtained from the slope using Equation 2. The value of $K_c^{(1)}$ is then substituted into Equation 2 with $Y = Y(\Delta a^{(0)})$ and the fracture stress of an unnotched specimen. This leads to a new value of Δa which is denoted $\Delta a^{(1)}$. This process is repeated until $K_c^{(n+1)} = K_c^{(n)}$ which generally requires five to eight iterations. The series of K_c values generated for set E is given in Table II together with the Δa values. The final value of K_c obtained was 0.20 MPa m$^{1/2}$ with $\Delta a = 1.2$ mm.

TABLE II The series of stress intensity factors and associated Δa values for set E obtained by iteration

n	0	1	2	3	4	5	6
$K_c^{(n)}$ (MPa m$^{1/2}$)	0.169	0.183	0.191	0.196	0.199	0.201	0.202
$\Delta a^{(n)}$ (mm)	0.770	0.936	1.040	1.107	1.156	1.180	1.201

It is now possible to determine the influence of incorporating Δa into the computation of the strain energy release rates. The crack initiation data will be considered first. According to Equation 5, there should be a linear relationship between U_i and $BD\phi$ if G_{ci} is a materials constant. Fig. 5 compares the appropriate data for $\phi = \phi(a)$ and $\phi = \phi(\tilde{a}^{(6)})$. It can be seen that the use of Δa linearizes the data; the calculated value of G_{ci} from the slope is 27.0 J m^{-2}

As might be expected, the effect of using $\tilde{a}$ instead of a to compute G_{cp} from Equation 6 is relatively small. Fig. 6 shows the appropriate plot of U_p as a function of $(D - a)$ and $(D - \tilde{a}^{(6)})$. In this case the value of G_{cp} is increased from 26.0 to 30.1 J m^{-2}

Finally for set E it is possible to compare the value of G_{ci} obtained above with that calculated from the iterated value of K_c using Equation 4. The elastic modulus measured for this set was 1.76 GPa and a Poisson's ratio of 0.2 was assumed for these relatively porous materials. The calculated value $(G_{ci})_{calc}$ is then 24.4 J m^{-2} which is in reasonable agreement with the value of 27.0 J m^{-2} obtained from the initiation energies.

The data for all the sets is given in Table I. The mean values of the propagation strain energy release

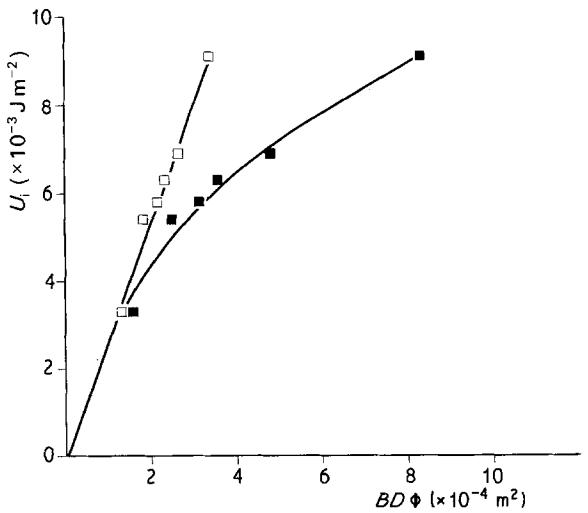

Figure 5 The initiation fracture energy U_i for set E as a function of $BD\phi$ where for ■ $\phi = \phi(a)$ and for □ $\phi = \phi(\tilde{a}^{(6)})$.

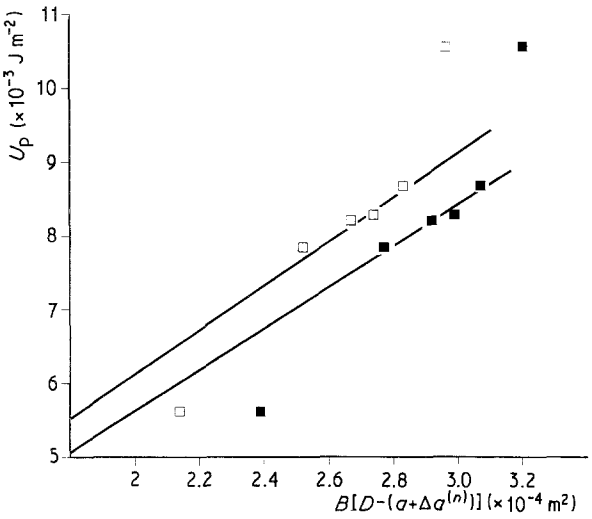

Figure 6 The propagation fracture energy U_p for set E as a function of $B(D - a)$ or $B(D - \tilde{a}^{(6)})$ which correspond to the symbols ■ and □ respectively.

rates $G_{cp}^{(0)}$ are generally about a factor of two higher than the corresponding initiation values $G_{ci}^{(0)}$. The iteration procedure leads to a much closer agreement between these two quantities. The strain energy release rates $(G_c)_{calc}$ calculated from $K_c^{(n)}$ are equal within experimental error to the $G_{ci}^{(n)}$ values. This shows the internal consistency of the procedure for the calculations based on forces or energy.

The Δa values are all of the order of 1 mm and do not appear to be related to the composition–porosity of the bars unlike the other parameters. The magnitudes of E, K_c and G_c are very sensitive to porosity as is well established for materials of this type (e.g. [12]). The bars all become stiffer or stronger as the concentration or molecular weights of the binder are increased. The effect of molecular weight is consistent with the rapid increase in toughness with molecular weight above a value of about 10^5 [13]. The bars containing a mixture of particle sizes are also stiffer and stronger than those from a single sieve fraction even though they were fabricated to have similar porosities. Generally, a wide particle size distribution increases the strength due to a reduction in porosity.

4. Discussion

It appears that the use of the quantity Δa allows LEFM to be applied to the type of porous particulate solids studied in the current work. Hence we will consider the interpretation of this quantity on the basis of previous fracture studies of particulate solids.

The simplest interpretation is that Δa represents a natural flaw size which is characteristic of the material. This interpretation was advocated by Birchall *et al.* [14] who measured the flexural strength of Portland cement paste as a function of notch size. It was found that the strength became independent of the notch size at about 1 mm which is similar to the values of Δa reported here. No attempt was made in this work to determine if the conditions for a linear analysis were applicable.

If Δa is a flaw size, it is difficult to envisage what this represents structurally since analytically it is obtained as the equivalent of a through-thickness notch. The composition–porosity range investigated has been sufficient to produce a greater than an order of magnitude change in the fracture parameters while the Δa values obtained were relatively insensitive and do not correlate with these changes. The load bearing elements in the bars are at the interparticle junctions formed by the polymer. It might be expected that Δa would correspond to some mean depth of junctions below the specimen surface that would be characterized by a relatively constant and small number of particle diameters rather than the wide range (2 to 17) observed.

An alternative to treating Δa as a pre-existing flaw is to consider the possibility of sub-critical crack growth which would produce a similar result. The conditions are very favourable for such an effect since there will be high stress concentrations at the interparticle junctions. In addition, sub-critical crack growth in ceramics has been widely reported (e.g. [15]). However, this is unlikely to be the case here since the crack extension would be a function of a/D and there would be a significant deviation of the load–deflection curves from a linear elastic response [15]; these conditions do not correspond to those observed in the current work.

Sub-critical crack growth would produce the same effect as that observed with pre-cracked ceramic specimens where it has been found that there is an increasing crack resistance curve [16]; that is K_{ci} increases with crack length as in the present work. However, this effect was not observed for notched specimens. It has been shown that the data for ceramics could be explained in terms of frictional stresses developed at the rear of the crack tip [17]. In this case it has been found that constant R curves can be obtained by introducing negative values of Δa to obtain the effective crack size [18]. This is the converse of what is found here. It might also be added that these frictional constraints are associated with G_{cp}/G_{ci} ratios being less than unity [19] which again is not in accordance with the present results.

Finally, we need to consider the possibility of Δa representing a process zone ahead of the crack tip. A special type of zone has been postulated for hardened cement paste which involves fibres stabilizing the crack front [4]. This was analysed using an analogy to the Dugdale model [20] and was thought to account for the fracture mechanics parameters being a function of specimen size. However, a more appropriate process zone for the current materials might be of the type envisaged for ceramics.

A process zone in a particulate solid can be defined as a volume of material where microcracking precedes the main crack front. This can have the effect of increasing the fracture energy by crack branching [21]. The origin of microcracking in ceramics is thought to be due to the high internal stress concentrations which developed during cooling [12]. Similar stresses would be generated in the present system due to the drying of the binder.

Measurements on ceramics have shown that generally the elastic modulus is proportional to the fracture energy (equal to $G_c/2$) [22] except for cases where microcracking increases the toughness and hence the

TABLE III Typical mechanical data for ceramics, polymers and the sand–PVP material studied in the present work

Material	K_c (MPa m$^{1/2}$)	G_c (J m^{-2})	E (GPa)	G_c/E (m)
Ceramics	4	40	350	1×10^{-10}
Polymers	4	4000	2	2×10^{-6}
Sand–PVP	0.2	20	2	1×10^{-8}

ratio G_c/E which can be regarded as some critical displacement (see later). The materials studied in the present work can be regarded as being intermediate between ceramics and polymers so that it is of interest to compare the mechanical properties. Typical values are given in Table III which suggests that indeed the critical displacement in the process zone is intermediate between the component materials of the sand–PVP bars. However, plastic zone sizes in polymers of about 1 mm are not uncommon. In the sand–PVP bars any displacement is confined to the junctions since the sand is relatively rigid. It is therefore not unreasonable to have a process zone size comparable to polymers but with the displacement involved being very much smaller.

The actual values of the ratio G_c/E are given in Table IV. The values for sets A, B, D and E are very similar; these correspond to those sets with monosize particles and the PVP binder with an MW of 7×10^5. Set C shows a lower G_c/E ratio which presumably corresponds to the much lower energies required to fracture junctions formed from the lower molecular weight brittle binder. The mixed particle size sets F and G appear to have characteristically lower G_c/E ratios.

The magnitude of the ratios G_c/E are related to the crack opening displacement δ by the following relationship

$$\delta = G_c/\lambda E \quad (7)$$

where λ is the yield strain which is typically 0.1 for polymers. This would produce δ values of the order of 0.1 μm which is extremely small if Δa represents a plastic zone analogous to that formed in polymers.

5. Conclusions

For porous particulate solids comprising of sand and a low phase volume of a polymeric binder it has been shown that a LEFM analysis can be applied if an effective crack length is used in a similar way to that widely applied to ductile materials having a limited plastic zone. The effective crack length is given by the sum of the notch depth a and a quantity Δa. This quantity is not sensitive to composition or porosity unlike the stiffness and fracture parameters. If Δa represented a natural flaw size it might be expected that it would have some dependence.

TABLE IV The ratios of G_c/E for the sand–PVP specimens

Set	A	B	C	D	E	F	G
G_c/E (10^{-8} m)	1.56	1.50	0.74	1.47	1.49	0.52	0.48

The behaviour of the materials studied here do not appear to be analogous to dense particulate solids such as ceramics or cement. The application of LEFM to these materials poses special problems which have not been observed in the present work. A possible interpretation of Δa is that it corresponds to a process zone ahead of the crack tip. The critical displacement in this zone is intermediate between ceramics and polymers. In the former, the process zone is a region where microcracking occurs while in polymers the plastic zone is associated with ductile yielding. It is possible for the present materials that energy is dissipated by either/or a mixture of such processes.

References

1. N. CLAUSSEN and J. JAHN, *Powder Met. Int.* **2** (1970) 87.
2. H. E. N. HIESTAND and D. P. SMITH, *Powder Tech.* **38** (1984) 145.
3. C. E. CAPES, "Particle Size Enlargement" (Elsevier, Amsterdam, 1980).
4. D. D. HIGGINS and J. E. BAILEY, *J. Mater. Sci.* **11** (1976) 1995.
5. H. WIENINGER, K. KROMP and R. F. PABST, *ibid.* **21** (1986) 411.
6. R. W. DAVIDGE and G. TAPPIN, *ibid.* **3** (1968) 165.
7. "Methods of Test for Plane Strain Fracture Toughness of Metallic Materials", BS 5447 (British Standards Institute, 1977).
8. D. P. ROOKE and D. J. CARTWRIGHT, "Compendium of Stress Intensity Factors" (HMSO, London, 1976).
9. J. M. KRAFFT, A. M. SULLIVAN and R. W. BOYLE, Crack Propagation Symposium, Cranfield, 1961, Paper 1.
10. G. R. IRWIN, "Handbuch der Physik", Vol. VI (Springer, Heidelberg, 1958).
11. E. PLATI and J. G. WILLIAMS, *Polym. Engng Sci.* **15** (1975) 470.
12. F. E. BURESCH, in "Fracture Mechanics Applied to Brittle Materials", Proceedings of the 11th National Symposium on Fracture Mechanics, Part II (ASTM, Philadelphia, 1979) p. 151.
13. P. PRENTICE, *J. Mater. Sci.* **20** (1985) 1445.
14. J. D. BIRCHALL, A. J. HOWARD and K. KENDALL, *Nature* **289** (1981) 388.
15. H. HUBNER and W. JILLEK, *J. Mater. Sci.* **12** (1977) 117.
16. R. F. PABST, J. STEELS and N. CLAUSSEN, "Fracture Mechanics of Ceramics", Vol. 4, edited by R. C. Bradt, D. P. H. Hasselman and F. F. Lange (Plenum Press, New York, 1978) p. 821.
17. H. WIENINGER, K. KROMP and R. F. PABST, *J. Mater. Sci.* **21** (1986) 411.
18. A. BORNHAUSER, K. KROMP and R. F. PABST, *ibid.* **20** (1985) 2586.
19. U. L. F. ENGEL and H. HUBNER, *ibid.* **13** (1978) 2003.
20. D. S. DUGDALE, *J. Mech. Phys. Solids* **18** (1960) 100.
21. C. CM. WU, S. W. FREIMAN, R. W. RICE and J. J. MECHOLSKY, *J. Mater. Sci.* **13** (1978) 2659.
22. J. J. MECHOLSKY, S. W. FREIMAN and R. W. RICE, *ibid.* **11** (1976) 1310.

Received 9 May
and accepted 12 September 1988